Electrowetting in Carbon Nanotubes
J. Y. Chen, *et al.*
Science **310**, 1480 (2005);
DOI: 10.1126/science.1120385

Science (print ISSN 0036-8075; online ISSN 1095-9203) is published weekly, except the last week in December, by the American Association for the Advancement of Science, 1200 New York Avenue NW, Washington, DC 20005.

Electrowetting in Carbon Nanotubes

J. Y. Chen, A. Kutana, C. P. Collier,* K. P. Giapis*

We demonstrate reversible wetting and filling of open single-wall carbon nanotubes with mercury by means of electrocapillary pressure originating from the application of a potential across an individual nanotube in contact with a mercury drop. Wetting improves the conductance in both metallic and semiconducting nanotube probes by decreasing contact resistance and forming a mercury nanowire inside the nanotube. Molecular dynamics simulations corroborate the electrocapillarity-driven filling process and provide estimates for the imbibition speed and electrocapillary pressure.

The long inner hollow core of carbon nanotubes offers opportunities for the study of fluid flow in nanoconduits (*1*), chemical reactions in nanosize test tubes (*2*), and electronic and magnetic behavior in encapsulated nanowires (*3*, *4*). Several methods have been devised to fill nanotubes with metals (*3*–*5*) and other materials (*6*–*11*), resulting mostly in the formation of discontinuous nanowires.

Capillarity has been shown to drive wetting and filling of carbon nanotubes with liquids, provided that the surface tension of the liquid is less than ~180 mN/m (*10*, *11*). Most pure metals, which possess surface tension greater than 200 mN/m, cannot be incorporated spontaneously into nanotubes, thus hindering the fabrication of metal nanowires by this simple method (*7*, *9*). Because liquid mercury was shown not to wet carbon nanotubes (*10*), immersion into mercury has served to provide a good Ohmic contact for measuring the electrical properties of individual nanotubes attached to scanning probe tips (*12*–*14*). Such measurements, however, can be affected by the application of an electrical potential across the nanotube-mercury interface, which can lower the surface tension and cause electrowetting (*15*). We now show that electrically activated wetting of carbon nanotubes is indeed possible, with important implications for nanofluidics, nanoprobes, nanowires, and controllable manipulation at the nanoscale.

Single-wall carbon nanotubes (SWNTs) were grown by chemical vapor deposition on a silicon wafer decorated with iron nanoparticles (*16*). We attached these SWNTs to gold-coated silicon atomic force microscope (AFM) tips to form "nanotube probes" using the pickup technique of Hafner *et al*. (*17*). Picked-up SWNTs with suspended length between 200 to 600 nm were selected for further processing. The tubes had an average diameter (±SD) of 5 ± 1 nm, larger than those (1 to 3 nm) reported by Hafner *et al*. (*17*) and were defect-free, as inferred from transmission electron microscopy (TEM) images.

After annealing for 36 hours at 180°C, each nanotube probe was subjected to electric pulse etching (1.5 to 3.5 V for 20 μs) against a fresh highly oriented pyrolytic graphite surface, as described elsewhere (*16*, *17*). The etching shortened the SWNT (to between 50 and 200 nm), which reduced bending and buckling effects and opened up its suspended free end to facilitate access of its inner core by wetting.

In ambient conditions, the shortened SWNT probe was brought into contact with a fresh droplet of liquid mercury (diameter of ~200 μm) by engaging the probe in tapping mode on the droplet surface with a Digital Instruments AFM and a Nanoscope IV controller. Both the total length of the SWNT and the length immersed in the mercury drop could be determined (*18*). Precautions were taken to prevent the gold-coated silicon tip from contacting the mercury surface directly because mercury dissolves the gold, causing nanotube loss. After the SWNT was immersed into Hg by 17 ± 2 nm, electrical dc potentials were applied to the nanotube probe while tip conductance was monitored (with the Hg at ground). Resistances were measured at low bias (100 mV). Two types of experiments were performed. For a fixed-probe position, current-voltage (*I-V*) curves were recorded. Alternatively, the SWNT was lifted from the mercury surface at fixed applied potential in order to measure the pull-off force acting on the tip.

Typical *I-V* curves for shortened nanotube probes are shown in Fig. 1. Initially, low currents (2 to 10 μA) were measured for potentials between +1 to –1 V (curve I to II). The probe of Fig. 1A has a low bias resistance of 208 ± 20 kilohms, consistent with the range of values reported for good contact between metallic SWNTs and gold-coated AFM tips (*13*). The probe of Fig. 1B has a resistance of 1.65 ± 0.29 megohms and a slightly asymmetric *I-V* curve (I to II), both indicative of a semiconducting SWNT. Probe resistances from a large number of metallic SWNTs ranged from 100 to 300 kilohms, with no apparent correlation with the length of the truncated SWNT (table S1). Semiconducting SWNTs had substantially higher resistances (1 to 3 megohms). The *I-V* curves were stable with voltage cycling between –1 and +1 V.

Increasing the voltage to a threshold value between ±1 and ±2 V while keeping the nanotubes immersed in the mercury at fixed depth led to an abrupt and large increase in conductivity (curve II to III), for both the metallic and semiconducting SWNTs. The jump to high current (termed "probe activation") occurred at –1.15 V for the metallic SWNT probe (Fig. 1A). Further increase in the magnitude of the applied voltage to –1.50 V caused a slight variation in current. Subsequent cycling of the voltage between ±1.5 V results in stable *I-V* curves at elevated currents (curves III to IV) for 10 to 15 cycles. The low bias resistance of the metallic SWNT probe in its activated state decreased to 29 ± 4 kilohms. The semiconducting SWNT probe exhibited a similar response (Fig. 1B); probe activation occurred at –1.26 V and its resistance dropped to 46.8 ± 2.9 kilohms, notably near the value for the activated metallic SWNT in Fig. 1A.

In addition to negative potentials, probe activation also occurs consistently at similar (absolute) positive potentials (fig. S1). For

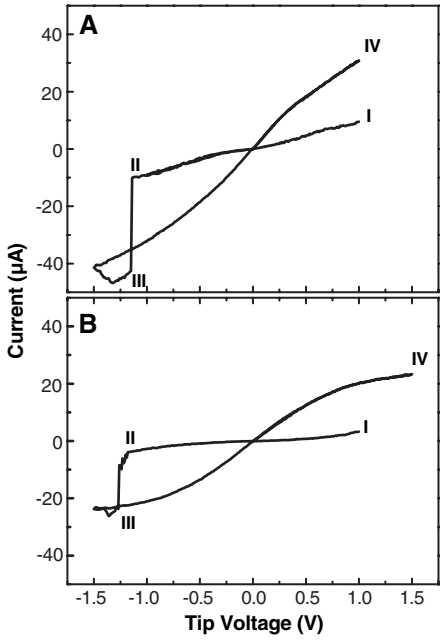

Fig. 1. Probe current as a function of applied tip voltage for (**A**) an 80-nm-long metallic SWNT and (**B**) a 130-nm-long semiconducting SWNT. Both nanotubes are immersed by 17 ± 2 nm into a mercury droplet. Curve I to II corresponds to the low-conductivity state. Curve II to III indicates the abrupt transition to the high-conductivity state, which is described by curve III to IV.

Division of Chemistry and Chemical Engineering, California Institute of Technology, Pasadena, CA 91125, USA.

*To whom correspondence should be addressed. E-mail: collier@caltech.edu (C.P.C.); giapis@cheme.caltech.edu (K.P.G.)

negative voltage sweeps, average activation thresholds were –1.5 ± 0.5 V for metallic and –1.3 ± 0.3 V for semiconducting SWNTs. After activation, and so long as the SWNT tip remained immersed, the high-conductivity behavior was maintained upon voltage cycling through zero bias, although a drift to higher resistances was seen at longer times (>5 min). When the SWNTs were completely removed from the mercury surface, they reverted to a low-conductivity state (*19*), although the corresponding resistance was generally lower than that before the first round of activation (table S1). The probe could be reactivated at a lower voltage than the initial threshold established previously; the high-conductivity state was then fully recovered.

Simultaneous measurement of the tip pull-off force from numerous force-distance curves with tip voltage indicated that probe activation coincides with a roughly fivefold increase in the attraction between the SWNT probes and mercury (Fig. 2A). This trend was consistent and readily observable for both metallic and semiconducting SWNTs (Fig. 2B). Relatively weak pull-off forces between 1 to 5 nN were measured before activation, as compared with strong forces of 11 to 30 nN after activation.

We attribute these observations to electrically activated wetting and filling of our SWNTs by mercury. Electrowetting has been demonstrated in microchannels (*15*) but not at the nanoscale. Also known as electrocapillarity, the effect is based on electrostatic control of the solid-fluid interfacial tension (*20*). After the application of a potential, charge builds up across the SWNT-mercury contact (*21*). The repulsion between similar electric charges present at the mercury surface lowers the surface tension (*22*). At a critical value of the applied potential, wetting may commence that forces mercury up along the SWNT sidewalls and also fills the SWNT core to form a continuous metallic nanowire. Mercury transported in this manner to the AFM tip can react with the gold to form an amalgam, which will alter the upper contact characteristics. Pumping enough mercury along the SWNT walls or through its core may even liquefy the upper contact and detach the SWNT from the tip.

These hypotheses led us to look for evidence of mercury trapped inside the activated SWNTs and/or gold coating loss from the AFM tip. We examined more than 50 activated SWNTs by ex situ TEM for evidence that mercury had penetrated and filled the inner core (*23*). Finding such evidence was difficult because extraction of the SWNT tip from the mercury surface effectively terminates electrowetting and allows mercury to evaporate. Nevertheless, we found two instances with clear evidence of material trapped inside the SWNT. The first case pertains to a 150-nm-long SWNT, a segment of which is visible in Fig. 3A along the sidewall of the AFM tip. Darker material inside the SWNT formed a highly curved meniscus with a contact angle of 150° ± 5°, notably close to that of mercury on graphite (*24*). Focusing the TEM electron beam on this material caused it to vanish but left behind a faint trace of the curved interface (Fig. 3B). We hypothesize that the material inside was liquid mercury in its nonwetting state and that heating from the electron beam made it move or evaporate rapidly, rendering its identification impossible.

The second case of TEM evidence for material inside an activated SWNT is presented in Fig. 4A. The contrast is sufficient to discern a darker material in the center of the lower half of the SWNT. Readily apparent in Fig. 4B is the dissolution of the gold-coating at the AFM tip apex, which exposes the silicon tip. Although this tip did not touch the mercury surface, its appearance is identical to that of a coated tip without a SWNT (Fig. 4C) that had been briefly immersed into mercury deliberately. Mercury must have been transported to the tip by some other mechanism. We considered four possibilities: evaporation, thermomigration, electromigration, or electrowetting. Mercury evaporation at room temperature requires long times (>15 hours) to dissolve 40-nm-thick gold films (*25*) and must be excluded. In the absence of wetting, thermomigration (*26*) would compete against surface tension (*27*). Electromigration is polarity dependent (*28*), whereas the phenomenon we describe here is not. Thus, the only plausible mechanism for mercury transport from the drop to the AFM tip is electrowetting.

We have performed molecular dynamics simulations (*18*) of SWNTs interacting with a mercury bath to help visualize the wetting process. Lippmann's model of electrowetting (*20*) was adopted for a cylindrical capacitor, defined between the nanotube and a column of mercury, with a potential V applied across the plates (*21*). When a neutral Hg atom is brought to the interface from the bulk of the liquid, the surface charge is redistributed over a greater area because of electrostatic repulsion. The free energy of the interface is then lowered by

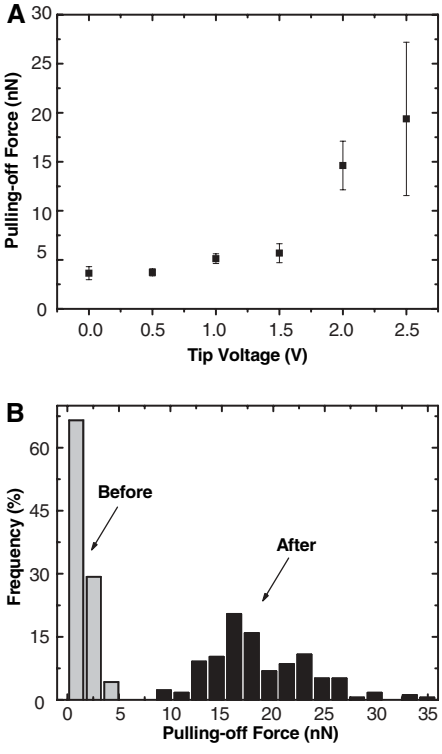

Fig. 2. (**A**) Pull-off force as a function of applied tip voltage for a 120-nm-long semiconducting carbon nanotube. The force is measured by extracting the nanotube from the mercury surface at the corresponding voltage. Error bars show means ± SD. (**B**) A histogram of pull-off forces measured by using 14 different SWNT probes. The "before-activation" region corresponds to 188 force-distance curves from six nanotubes recorded at a tip bias of 0 V. The "after-activation" region corresponds to 176 force-distance curves from eight nanotubes, recorded at a tip bias of ±2 V.

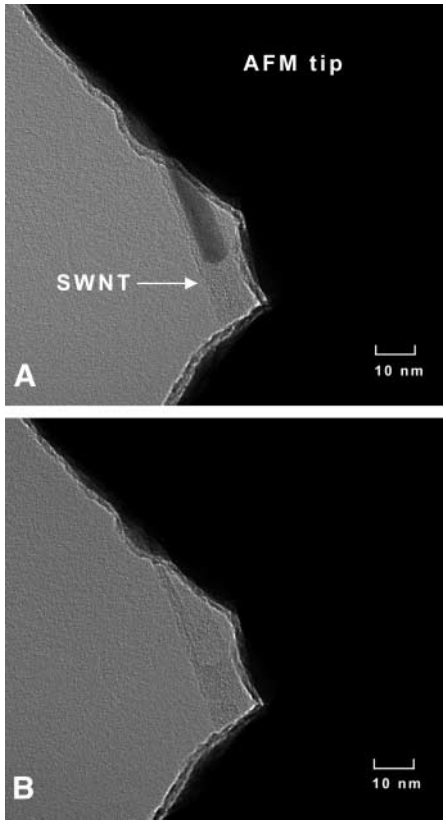

Fig. 3. (**A**) Transmission electron micrograph of a segment of an activated 150-nm-long SWNT attached on a gold-coated AFM tip. Material of darker contrast fills the upper core of the nanotube, forming a highly curved meniscus with a contact angle of 150° ± 5°. (**B**) The same region after focusing the TEM electron beam on the material inside the nanotube. A faint trace is left behind at the position of the meniscus.

an amount equal to the change ΔE_e in electrostatic energy:

$$\Delta E_e = -cV^2/2\rho_s \quad (1)$$

where $c = C/A$ is the capacitance per unit area and $\rho_s = 11.82\ \mathrm{nm}^{-2}$ is the surface density of mercury. The energy drop was realized through a local external force acting along the surface normal on each atom near the interface according to:

$$F_{ext}(r) = \begin{cases} F_0, & 0 < r < a \\ 0, & r \geq a, r \leq 0 \end{cases} \quad (2)$$

where r is the normal distance to the surface, $a = 3.5$ Å is a characteristic distance, and $F_0 = \Delta E_e/a$. The direction of the force is toward the surface, and a is chosen to include atoms from the second surface layer. Although a simplification, this model contains the salient features of electrowetting and should give a reasonable description of its dynamics.

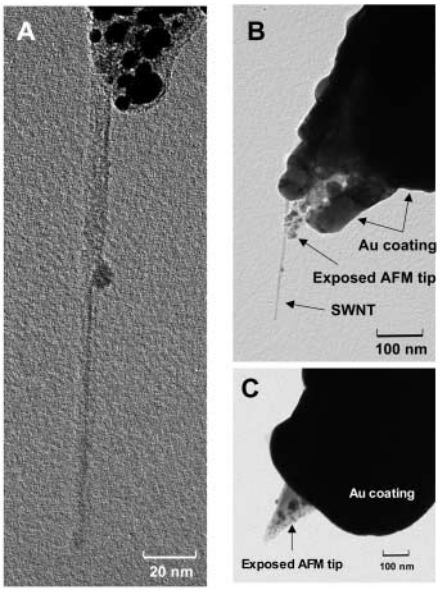

Fig. 4. (**A**) Transmission electron micrograph of an activated 180-nm-long SWNT attached to a gold-coated AFM tip. Material of darker contrast fills the lower half portion of the nanotube core. The material appears to terminate near a bulge or particle on the outside of the nanotube. The position of the bulge coincides with the outer edge of the coating before removal. Beyond the bulge, the nanotube diameter appears to be larger, suggesting the presence of a second nanotube terminating at the bulge. (**B**) Zoom-out of micrograph (A), indicating that the gold-coating at the AFM tip apex has been dissolved by mercury (leaving separated domains of AuHg amalgam on the Si tip), although no direct contact with the mercury surface has been made. (**C**) Micrograph of a different gold-coated AFM tip without a nanotube, which has been dipped into mercury deliberately to expose the Si tip apex by gold dissolution.

Simulating long (40,40) SWNTs, near the size of the experimental ones, with correspondingly large mercury baths was computationally prohibitive. Instead, we simulated (*29*) the immersion of a 15.7-nm-long uncapped (20,20) SWNT in a configuration similar to that suggested by Supple and Quirke (*30*). In the equilibrium state of an immersed SWNT without applied voltage, a nonwetting meniscus forms on the outside and mercury does not penetrate the open unblocked end (Fig. 5A). For the same nanotube 1.5 ns after the application of 3.5 V, which is larger than the calculated threshold of 2.5 V for electrowetting (*31*), mercury has filled the core and wetted the outside walls (Fig. 5B). Indeed, wetting begins immediately after the potential is turned on and the liquid moves inside as a single front at a speed of ~13 m/s, whereas a thin film spreads on the outer wall. Of course, a closed SWNT capped at the free end would only be wetted at the outside (fig. S4).

The mass-transport rate of Hg atoms through the SWNT core depended quadratically on the applied potential (fig. S5), a scaling that deviates from the linear dependence predicted by the Lucas-Washburn equation for filling of macroscopic capillaries (*30*, *32*). At an applied voltage of 3.5 V, the imbibition speed of mercury is 2.7×10^{12} atoms per second. An estimate (*33*) of the amount of Au (1.55×10^8 atoms) dissolved from the AFM tip of Fig. 4B suggests that the Hg transport rate is more than sufficient to account for the removed Au. The electrocapillary pressure (ECP) was also calculated to have a quadratic dependence on applied potential (fig. S6), in agreement with observations in microchannels (*15*). Typical ECP calculated values are in the range of 0 to 3 kbar (for potentials between 2.5 and 4.5 V), indicating a large driving force for wetting.

The simulations offer a starting point for explaining experiments. Electrowetting is an activated process with a threshold voltage. Once that voltage is exceeded, mercury imbibes into the SWNT core and is also transported along the outer sidewalls, rapidly reaching the Au-coated AFM tip, where it reacts with gold to form an amalgam. As more Hg arrives, the upper contact is liquefied and becomes more similar to the lower SWNT-Hg contact, that is, more Ohmic (*13*). The voltage drop across the upper contact decreases, which increases the applied potential across the lower contact. This high potential, in turn, increases the ECP and the Hg transport rate to the AFM tip. Thus, the observed improvement in conductance is a result of better wetting at the lower contact, changes in the upper contact in response to the supply of Hg, and the formation of a column of Hg in the SWNT core.

Experiments with SWNTs that have not undergone pulsed etching and are believed to be closed consistently exhibit larger electrowetting thresholds and never reach the high levels of conduction seen with open SWNTs. This observation suggests that the Hg column that forms in the SWNT core must contribute to the lowering of the probe resistance. Indeed, in one case of a 270-nm-long individual SWNT, we measured an activated probe resistance of 3.79 ± 0.18 kilohms (table S1), equivalent to four times the conductance quantum $G_0 = (12.9\ \text{kilohms})^{-1}$. In addition, the metal-filled core may be responsible for the marked increase in conductance of initially semiconducting SWNTs upon probe activation.

When nanotubes are removed from the mercury surface, electrowetting ceases, and the inner Hg column rapidly disintegrates by draining (*34*) and evaporation because wetting is no longer supported. Once Hg is no longer supplied to the upper contact, the remaining Hg diffuses into the surrounding Au to form a solid AuHg amalgam. This amalgam at the upper contact has a lower work function than pure Au (*35*), resulting in probe activation at

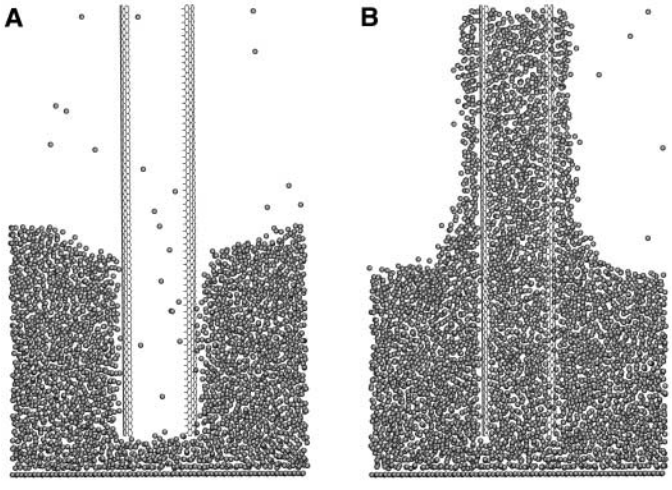

Fig. 5. Results from molecular dynamics simulations of a 15.7-nm-long (20,20) SWNT immersed into a mercury bath at 300 K (**A**) before (at time zero with no applied bias) and (**B**) after probe activation (1.5 ns after application of a potential of 3.5 V).

a reduced threshold voltage upon reimmersion. Electrowetting is by definition an attractive interaction between mercury and SWNT and, thus, the force required to pull a SWNT off a mercury surface should be larger in an activated state than that of a nonactivated state (*36*).

Electrowetting in carbon nanotubes may offer opportunities for studies of nanofluidic transport. It can also be exploited for the formation of continuous nanowires crystallized in one dimension from low–melting point metals (e.g., Ga and In), enabling the measurement of the intrinsic electrical and magnetic properties of encapsulated nanowires. Such structures, attached to AFM tips, could serve as robust nanoelectrode probes with increased current load capacity and enhanced imaging capabilities.

References and Notes

1. Y. Gogotsi, J. A. Libera, A. Güvenc-Yazicioglu, C. M. Megaridis, *Appl. Phys. Lett.* **79**, 1021 (2001).
2. D. Ugarte, A. Chatelain, W. A. de Heer, *Science* **274**, 1897 (1996).
3. P. M. Ajayan, S. Iijima, *Nature* **361**, 333 (1993).
4. C. Guerret-Plecourt, Y. Le Bouar, A. Loiseau, H. Pascard, *Nature* **372**, 761 (1994).
5. C. H. Kiang, J. S. Choi, T. T. Tran, A. D. Bacher, *J. Phys. Chem. B* **103**, 7449 (1999).
6. S. C. Tsang, Y. K. Chen, P. J. F. Harris, M. L. H. Green, *Nature* **372**, 159 (1994).
7. T. W. Ebbesen, *J. Phys. Chem. Solids* **57**, 951 (1996).
8. P. M. Ajayan, T. W. Ebbesen, *Rep. Prog. Phys.* **60**, 1025 (1997).
9. M. Monthioux, *Carbon* **40**, 1809 (2002).
10. E. Dujardin, T. W. Ebbesen, H. Hiura, K. Tanigaki, *Science* **265**, 1850 (1994).
11. E. Dujardin, T. W. Ebbesen, A. Krishnan, M. M. J. Treacy, *Adv. Mater.* **10**, 1472 (1998).
12. S. Frank, P. Poncharal, Z. L. Wang, W. A. de Heer, *Science* **280**, 1744 (1998).
13. N. R. Wilson, D. H. Cobden, J. V. Macpherson, *J. Phys. Chem. B* **106**, 13102 (2002).
14. P. Poncharal, C. Berger, Y. Yi, Z. L. Wang, W. A. de Heer, *J. Phys. Chem. B* **106**, 12104 (2002).
15. M. W. J. Prins, W. J. J. Welters, J. W. Weekamp, *Science* **291**, 277 (2001).
16. L. A. Wade, I. R. Shapiro, Z. Ma, S. R. Quake, C. P. Collier, *Nano Lett.* **4**, 725 (2004).
17. J. H. Hafner, C.-L. Cheung, T. H. Oosterkamp, C. M. Lieber, *J. Phys. Chem. B* **105**, 743 (2001).
18. Materials and methods are available as supporting material on *Science* Online.
19. To measure conductance, the probe is reimmersed into mercury and the current is measured at low bias (100 mV).
20. G. Lippmann, *Ann. Chim. Phys.* **5**, 494 (1875).
21. The exact mechanism of charge buildup at the SWNT-mercury interface is not known, but it is thought to be caused by a tunneling barrier to electrons in a direction perpendicular to the SWNT center axis (*37*).
22. N. K. Adam, *The Physics and Chemistry of Surfaces* (Dover, New York, 1968).
23. We never found any solid or liquid material inside as-grown nanotubes despite extensive TEM imaging of hundreds of nanotubes grown by our chemical vapor deposition technique.
24. A. Awasthi, Y. J. Bhatt, S. P. Garg, *Meas. Sci. Technol.* **7**, 753 (1996).
25. M. Fialkowski, P. Grzeszczak, R. Nowakowski, R. Holyst, *J. Phys. Chem. B* **108**, 5026 (2004).
26. R. E. Hummel, *Int. Mater. Rev.* **39**, 97 (1994).
27. After activation, the measured high currents suggest large power dissipation, most likely occurring at both contacts. Thermomigration is not expected to contribute appreciably to mass transport from the Hg bath to the AFM tip, if both contacts become hot.
28. B. C. Regan, S. Aloni, R. O. Ritchie, U. Dhamen, A. Zettl, *Nature* **428**, 924 (2004).
29. The Hg bath consists of 37,013 mercury atoms. Periodic boundary conditions are applied in the *x* and *y* directions, and the size of simulation domain is 10.8 by 10.4 nm. The liquid is positioned on top of a layer of fixed Hg atoms, and the SWNT is initially placed outside the bath. After equilibration at 300 K, the SWNT is lowered into the liquid at a constant speed of 10 m/s while the liquid is maintained at 300 K. Carbon-carbon interactions in the walls are omitted to decrease the time of computation.
30. S. Supple, N. Quirke, *Phys. Rev. Lett.* **90**, 214501 (2003).
31. We perform the calculation at a potential larger than the calculated threshold (2.5 V) for electrowetting of the (20,20) SWNT to speed up the wetting and filling. Calculated thresholds increase with nanotube diameter and are generally larger than those seen experimentally.
32. The quadratic scaling can be predicted through the Lucas-Washburn equation by introducing a velocity-dependent dynamic contact angle or, correspondingly, a "wetting-line friction" as proposed by Martic *et al*. (*38*).
33. To estimate the amount of the dissolved Au, we assume a pyramidal AFM tip with conformal Au coating, which terminates into a spherical apex. We also assume that 30% of the Au atoms in the remaining Au coating with the lighter contrast have formed an amalgam.
34. The simulation predicts that mercury will rapidly drain from the (20,20) SWNT core at a speed of 15 m/s when the applied potential is decreased to zero.
35. The work function of Au (5.1 eV) is greater than that of Hg (4.6 eV) and the amalgam value should be in between (*39*).
36. A nonwetting condition is always repulsive. The weak pull-off force measured at voltages below threshold must be a result of extraneous effects such as adsorbed water. It is important to focus on the difference in pull-off force before and after activation.
37. B. Shan, K. Cho, *Phys. Rev. B* **70**, 233405 (2004).
38. G. Martic *et al.*, *Langmuir* **18**, 7971 (2002).
39. H. B. Michaelson, *J. Appl. Phys.* **48**, 4729 (1977).

40. We thank C. Garland for TEM assistance. Supported in part by NSF (grants CTS-0404353 and CTS-0508096) and in part by the Arrowhead Research Corporation.

Supporting Online Material

www.sciencemag.org/cgi/content/full/310/5753/1480/DC1
Materials and Methods
Figs. S1 to S6
Tables S1 and S2
References

20 September 2005; accepted 1 November 2005
10.1126/science.1120385

A Well-Preserved *Archaeopteryx* Specimen with Theropod Features

Gerald Mayr,[1]* Burkhard Pohl,[2] D. Stefan Peters[1]

A nearly complete skeleton of *Archaeopteryx* with excellent bone preservation shows that the osteology of the urvogel is similar to that of nonavian theropod dinosaurs. The new specimen confirms the presence of a hyperextendible second toe as in dromaeosaurs and troodontids. *Archaeopteryx* had a plesiomorphic tetraradiate palatine bone and no fully reversed first toe. These observations provide further evidence for the theropod ancestry of birds. In addition, the presence of a hyperextendible second toe blurs the distinction of archaeopterygids from basal deinonychosaurs (troodontids and dromaeosaurs) and challenges the monophyly of Aves.

The Archaeopterygidae from the Late Jurassic of Germany are recognized as the earliest undisputed fossil avians (*1*, *2*). Archaeopterygids have been known from nine skeletal specimens (*3*, *4*), and most of these are fragmentary or poorly preserved. As a result, crucial features of their osteology have remained uncertain or entirely unknown (*3*, *5*).

Here we describe a 10th skeletal specimen of an archaeopterygid (*3*, *4*). The specimen was discovered in an unknown locality of the Solnhofen area and was housed in a private collection before it was recently acquired by the Wyoming Dinosaur Center, Thermopolis, USA (collection number WDC-CSG-100; a cast will be deposited in Forschungsinstitut Senckenberg).

The "Thermopolis specimen" is a slightly dissociated skeleton on a single slab of pure limestone. Wing and tail feather impressions are well preserved (Fig. 1). In size and osteology, the new specimen corresponds best with the Munich specimen, which is the holotype of *Archaeopteryx bavarica* (*6*) (table S1). However, because there is an ongoing controversy about the taxonomic composition of the Archaeopterygidae, which currently include two genera, *Archaeopteryx* and *Wellnhoferia* (*3*, *7*), we do not assign the new specimen to a particular species in the present study.

The skull is the best-preserved one of all archaeopterygids and the only one that is exposed in dorsal view. There are two accessory antorbital openings, which were recognized in the Eichstätt specimen but whose presence was recently questioned (*3*, *8*). They are part of the maxillary bone (*9*, *10*) and not

[1]Forschungsinstitut Senckenberg, Division of Ornithology, Senckenberganlage 25, D-60325 Frankfurt am Main, Germany. [2]Wyoming Dinosaur Center, 110 Carter Ranch Road, Post Office Box 912, Thermopolis, WY 82443, USA.

*To whom correspondence should be addressed. E-mail: Gerald.Mayr@senckenberg.de